electronics

MDPI

Article

Characterizing Lossy Dielectric Materials in Shock Physics by Millimeter-Wave Interferometry Using One-Dimensional Convolutional Neural Networks and Nonlinear Optimization

Ngoc Tuan Pham [1,2], Alexandre Lefrançois [3,*] and Hervé Aubert [1]

[1] Centre National de la Recherche Scientifique, Laboratoire d'Analyse et d'Architecture des Systèmes (CNRS-LAAS), Toulouse University, 7 Avenue du Colonel Roche, 31031 Toulouse, France
[2] Institut National des Sciences Appliquées (INSA) Centre—Val de Loire, 88 boulevard Lahitolle, 18000 Bourges, France
[3] Commissariat à l'Energie Atomique et aux Energies Alternatives—Direction des Applications Militaires (CEA-DAM), GRAMAT, BP80200, 46500 Gramat, France
* Correspondence: alexandre.lefrancois@cea.fr

Abstract: When a dielectric material undergoes mechanical impact, it generates a shock wave, causing changes in its refractive index. Recent demonstrations have proven that the modified refractive index can be determined remotely using a millimeter-wave interferometer. However, these demonstrations are based on the resolution of an inverse electromagnetic problem, which assumes that the losses in the material are negligible. This restrictive assumption is overcome in this article, in which a new approach is proposed to solve the inverse electromagnetic problem in lossy and shocked dielectric materials. Our methodology combines a one-dimensional convolutional neural network architecture, namely Inverse problem of Lossless or Lossy Shocked Wavefront Network (ILSW-Net), with a nonlinear optimization technique based on the Nelder–Mead algorithm to estimate losses within dielectric materials under a mechanical impact. Experimental results for both simulated and real signals show that our method can successfully predict the velocities and the refractive index while accurately estimating the shock wavefront.

Keywords: convolutional neural network; nonlinear optimization; shocked materials; lossy dielectrics; millimeter-wave interferometry; complex refractive index; shock wavefront velocity; particle velocity

Citation: Pham, N.T.; Lefrançois, A.; Aubert, H. Characterizing Lossy Dielectric Materials in Shock Physics by Millimeter-Wave Interferometry Using One-Dimensional Convolutional Neural Networks and Nonlinear Optimization. *Electronics* **2024**, *13*, 1664. https://doi.org/10.3390/electronics13091664

Academic Editors: Yue Wu, Kai Qin, Maoguo Gong and Qiguang Miao

Received: 18 March 2024
Revised: 21 April 2024
Accepted: 23 April 2024
Published: 25 April 2024

1. Introduction

This study focuses on the field of shock physics—in particular, targeting accurate estimation of the refractive index of dielectric materials under a mechanical impact using interferometry techniques. Such estimation remains challenging due to the large variation of the wave magnitude depending on the type of material.

To address this problem, existing works leverage either classic measurement-based [1–8] or data-driven [9] approaches to characterize properties of shocked dielectric materials. In detail, the method introduced by B. Rougier et al. [7,8] is based on the measurement of two specific Doppler frequencies in the waveform delivered by a millimeter-wave interferometer. This approach provided valuable information on the shock wavefront velocity and particle velocity in shocked dielectric materials, as well as estimation of the refractive index, supposing that material losses are negligible. In parallel, Ref. [9] makes use of a regression learning-based approach using a one-dimensional convolutional neural network (1D-CNN) to improve the estimation, even with a short-duration wavefront. However, the dielectric losses in materials are still neglected; therefore, it can only estimate the real part of the complex refractive index of the shocked dielectric materials.

Our work aims at overcoming the aforementioned limitation by adopting a novel deep learning framework capable of dealing with dielectric losses in materials. Compared

to the previous work reported in [9], our method is able to extend the outcome of the regression problem by retrieving both real and imaginary parts of the complex refractive index of shocked materials. This extension thus allows us to effectively address the impact of dielectric losses (a crucial aspect often neglected in previous studies) on the waveforms delivered by the millimeter-wave interferometer.

Our contributions are summarized as follows:

- A more robust 1D-CNN is proposed to address the inverse problem of lossless/lossy shocked wavefront (ILSW-Net), which embeds information about the complex refractive index of the material at rest to boost the prediction performance. The model's performance is empirically validated on simulated validation data, demonstrating ability to significantly reduce the prediction error.
- A physics-informed loss between the input signal and the approximated signal computed through the estimation of the velocities and the complex refractive index is introduced. Moreover, this loss is minimized using a nonlinear optimization technique, namely the Nelder–Mead algorithm, enabling estimation even in the case of experimental data in which the measured complex refractive index is unavailable. The results show out that the obtained approximated signal fits better with the original one, and the estimation error is reduced.

This paper is organized as follows. In Section 2, the proposed methodology of input/output data normalization (Section 2.1) is first described; then, the architecture of the ILSW-Net model (Section 2.2) is presented before introducing the nonlinear optimization algorithm used to minimize the physics-informed loss in the time domain (Section 2.3). Next, the setting for the learning process is described in Section 3, including the loss function and hyper-parameter configuration. In Section 4, the proposed model is compared with the model presented in [9], specifically focusing on lossless materials (Section 4.1). Following this, the performance of the method is reported for both simulated and experimental data delivered by a millimeter-wave (94 GHz) interferometer during a shock experiment involving High-Density Polyethylene (HDPE) and PolyMethyl Methacrylate (PMMA) materials for the case of lossy material (Section 4.2). Finally, conclusions and perspectives are presented in Section 5.

2. Proposed Method to Derive the Refractive Index of Lossy Dielectric Materials Subjected to Shock

2.1. Data Preprocessing

2.1.1. Normalization of the Signal Delivered by the Millimeter-Wave Interferometer during a Shock Experiment

A sample of lossy dielectric material of known thickness (d) and known complex refractive index (n_1) is considered here. When it is subjected to a mechanical impact, the complex refractive index of the material is modified. Let n_2 denote the complex refractive index modified by the shock. V_1 and V_2 denote the shock wavefront velocity and particle velocity, respectively. A millimeter-wave interferometer operating at 94 GHz is used here to remotely characterize the shocked material (see, e.g., [8]). During the shock experiment, the interferometer delivers a waveform in time-domain from which the complex refractive index (n_2) of the shocked material can be estimated.

The learning process of the proposed ILSW-Net utilizes simulated waveforms that are generated from the theoretical extension of [10,11] to account for losses in dielectric materials. The K waveforms ($s_k(t)$, where $k = 1, 2\ldots, 12{,}500$ and $t \leq 5$ µs) are approximately expressed as follows:

$$s_k(t) = \sum_{n=0,1,2,\ldots}^{\infty} A_n \cos\left(2nf_1 t - n2\pi f_2 t - \psi + \varphi_n\right) \quad (1)$$

with

$$f_1 \cong \frac{2V_1}{\lambda} r_1,\ f_2 \cong \frac{2(V_1 - V_2)}{\lambda} r_2,\ \psi \cong 2\pi \frac{2d}{\lambda} r_1,$$

$$A_n \cong \begin{cases} |R_{11}|e^{-\alpha d} \; if \; n = 0 \\ \left|T_{12}R_{22}^{n-1}T_{21}\right|e^{-\alpha d} \; if \; n > 0' \end{cases}$$

$$\varphi_n \cong \begin{cases} Arg(R_{11}) \; if \; n = 0 \\ Arg\left[T_{12}(-1)^n R_{22}^{n-1}T_{21}\right] \; if \; n > 0 \end{cases}$$

and

$$\lambda = \frac{c}{f},\ \alpha = 2\frac{2\pi}{\lambda}\kappa_1,\ R_{11} \cong \frac{n_1 - n_2}{n_1 + n_2},\ R_{22} \cong \frac{n_2 - n_1}{n_2 + n_1},\ \mathrm{T}_{12} \cong \frac{2n_2}{n_2 + n_1},\ \mathrm{T}_{21} \cong \frac{2n_1}{n_1 + n_2},$$

where λ designates the wavelength of the incident electromagnetic wave in vacuum; f is the operating frequency of the interferometer; c is the speed of light in vacuum; r_1 (>0) and r_2 (>0) are the value of the real part of refractive indexes n_1 and n_2, respectively; and κ_1(>0) and κ_2(>0) are the absolute value of the imaginary part (called absorption coefficient) of refractive indexes n_1 and n_2, respectively.

Before being used as the initial features (input) for the ILSW-Net model, the K waveforms ($s_k(t)$_ are normalized by $e^{-\alpha d}$, where α (>0) denotes the attenuation constant of the electromagnetic field in the lossy dielectric material at rest. The resulting normalized signal ($\widetilde{s}_k(t)$) used for the learning process is then given as follows:

$$\widetilde{s}_k(t) = s_k(t)/e^{-\alpha d} \;\text{ with } \alpha = \kappa_1 4\pi/\lambda \tag{2}$$

It is empirically observed that without the normalization of Equation (2), ILSW-Net struggles to effectively learn and generalize from the data (see Section 4.1). Indeed, as highlighted in Section 4, this preprocessing step ensures that the input data are appropriately scaled, facilitating the model's ability to discern patterns and relationships within the waveform data.

2.1.2. Normalization of Output Variables

In our approach, a single 1D-CNN is used to solve a linear regression problem with the following four outputs: the shock wavefront velocity (V_1), the particle velocity (V_2), and the real part (r_2) and the absolute value κ_2 of the imaginary part of the refractive index (n_2) of the shocked material. This problem involves predicting a continuous numeric output variable based on one or more input features. In this context, the min–max scaling procedure could be used to standardize the labeled output in the linear regression process. The normalized value (x_{scaled}) of parameter x is defined as follows:

$$x_{scaled} = (x - x_{\min})/(x_{max} - x_{\min}) \tag{3}$$

where x_{max} and $x_{\min}$ denote the maximum and minimum value within the dataset, respectively.

2.2. Architecture of ILSW-Net

A neural network architecture is introduced to tackle the inverse problem, i.e., retrieving V_1, V_2, r_2, and κ_2 from the lossy wavefront input signal. The primary goal is to manipulate the normalized waveform ($\widetilde{s}_k(t)$) in the time domain, where each time sample ($\widetilde{s}_k(t_n)$, where n = 1, 2, . . ., N) is assumed to be related to the unknown (complex) refractive index (n_2) of the shocked dielectric material.

Figure 1 shows the proposed ILSW-Net architecture dedicated to resolving the regression problem. It consists of two main parts, namely a convolutional feature extractor followed by a cascade of dense layers. The convolutional feature extractor is inspired by the residual network architecture [12] and influenced by the 1D ResNet model [13]. It receives the initial waveform of size 12,500 as input and learns discriminant features through the cascade of 1D convolutions and max poolings. Specifically, it makes use of two residual building blocks, namely a convolutional (Conv.) block and an identity (Iden.) block. the

Conv. block has two branches, in which the first branch contains a Conv1D and the second branch has 2 consecutive Conv1D layers, allowing feature learning at different receptive fields of 3 and 5. These features are then combined by an addition. In the case of the Iden. block, the first branch is simply the input of the block. At the end of the convolutional feature extractor, global average pooling is used to obtain a vector with a length of 384.

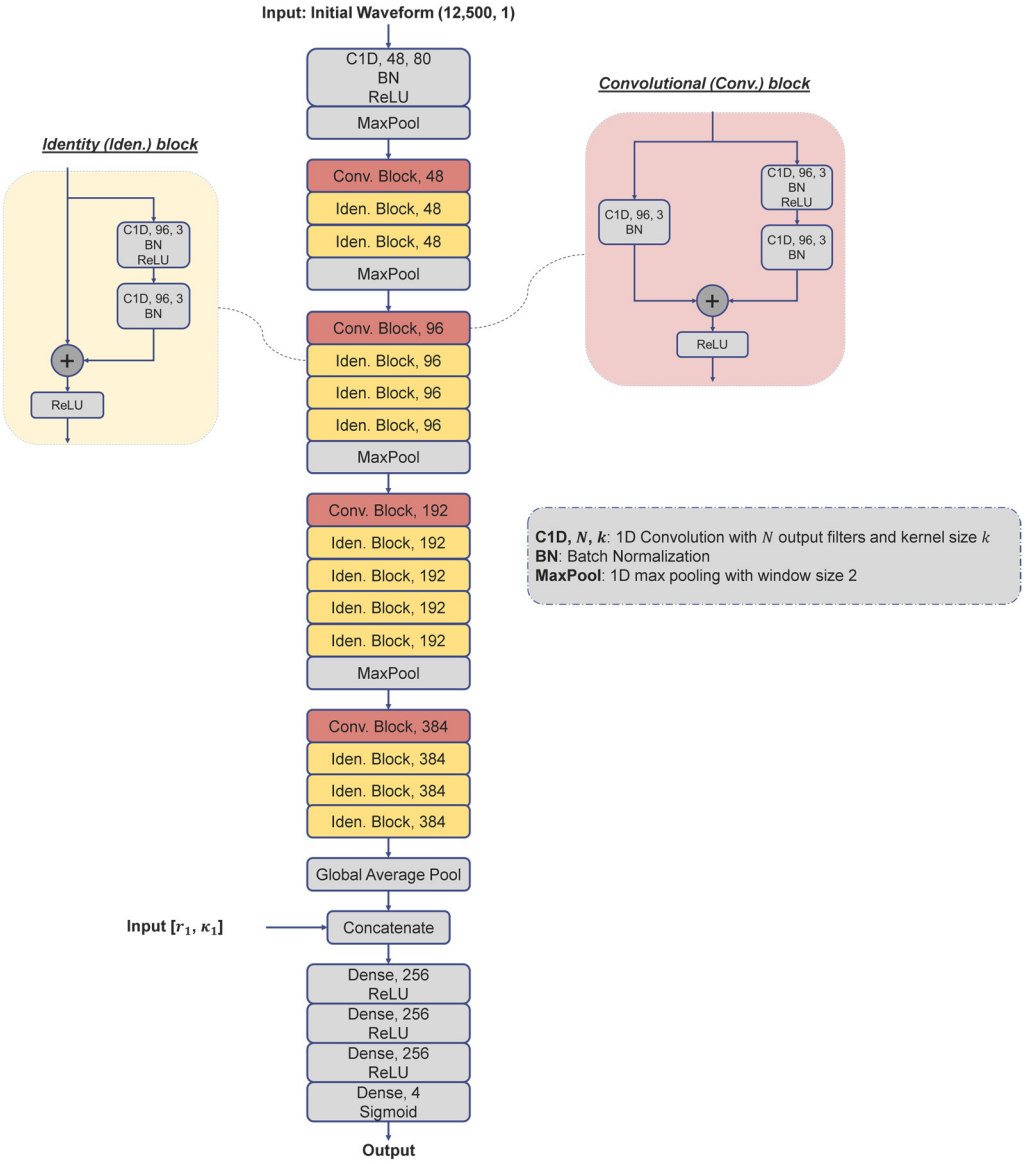

Figure 1. Architecture of ILSW-Net used to estimate the shock wavefront velocity (V_1), particle velocity (V_2), and the complex refractive index (n_2) of the shocked dielectric material from simulated waveforms. Note that using the complex refractive index (n_1) is a way to incorporate physical knowledge into the model, advantageously boosting its performance.

The second part is the fully connected regressor, aiming at estimating the following 4 outcomes: the shock wavefront velocity (V_1), particle velocity (V_2), and the real and imaginary parts of the refractive index (n_2). In particular, the known complex refractive index (n_1) of the material at rest is used by concatenating its real part and imaginary part with the features learned by the convolutional feature extractor. Including physical knowledge in the model is necessary for effective learning. Without the information provided by refractive index n_1, the model cannot learn the relationships between the input data and the output, leading to diminished performance. This is demonstrated in the next section.

2.3. Physics-Informed Loss and the Nelder–Mead Optimization Algorithm

Velocities V_1 and V_2 can be measured and/or calculated from the impact velocity with hydrocode shock behavior numerical simulations. However, there does not exist any method capable of precisely measuring the exact complex refractive index (n_2) using a radio-interferometer. Consequently, a simple confidence loss between the predicted and measured values of the complex refractive index (n_2) cannot be used in the case of experimental signals. Even when the model is well trained on a simulated dataset with available ground-truth values (V_1, V_2, r_2, κ_2), its performance on realistic data remains uncertain due to the absence of measured values of the complex refractive index (n_2). To address this issue, we employ a physics-informed loss to constrain matching between the reconstructed signal and the original experimental signal in the time domain. In particular, we make use of Equation (1) to obtain an approximated waveform from the predicted values of V_1, V_2, and n_2. Then, we compute the mean square error (MSE) loss between this approximated signal and the denoised original waveform as follows:

$$J(t_1,\ t_2,\ \ldots,\ t_n,\ \ldots\ t_N) = \frac{1}{N}\sum_{n=1}^{N}[\widetilde{s}_{sim}(t_n) - \widetilde{s}_{orig}(t_n)]^2 \tag{4}$$

where $\widetilde{s}_{sim}$ and $\widetilde{s}_{orig}$ denote the approximately simulated and denoised original waveforms, both normalized according to Equation (2). By minimizing this loss, we can ensure that the waveform derived from calculations fits well with the original realistic waveform. However, given the presence of complex numbers in Equation (1), this loss cannot be minimized by canonical gradient descent algorithms. Instead, the recently proposed Nelder–Mead algorithm [14] is employed, which is a versatile and robust numerical optimization technique widely used in various scientific and engineering applications.

3. Learning Procedure and Hyper-Parameter Setting

3.1. Learning Procedure

As mentioned above, a two-stage learning procedure is conducted to deal with both simulated and realistic signals taken from lossy materials. In the first stage, the ILSW-Net model is trained with a mean absolute error (MAE) loss computed between the predicted and ground-truth variables (V_1, V_2) and the real and imaginary parts of n_2 as follows:

$$\mathrm{L} = \frac{1}{4N}\sum_{n=1}^{N}\left|V_{1,n} - \hat{V}_{1,n}\right| + \left|V_{2,n} - \hat{V}_{2,n}\right| + \left|r_{2,n} - \hat{r}_{2,n}\right| + \left|\kappa_{2,n} - \hat{\kappa}_{2,n}\right| \tag{5}$$

where $V_{1,n}$ and $\hat{V}_{1,n}$ denote the original and predictive values of shock wavefront velocity V_1, respectively; $V_{2,n}$ and $\hat{V}_{2,n}$ designate the original and predictive values of particle velocity V_2, respectively; $r_{2,n}$ and $\hat{r}_{2,n}$ are the original and predictive values of the real part of refractive index n_2, respectively; and $\kappa_{2,n}$ and $\hat{\kappa}_{2,n}$ are the original and predictive values of the imaginary part (absolute value) of refractive index n_2, respectively. The training and validation datasets, comprising 10,000 signals for training and 2000 signals for validation, are generated via Equation (1). The dynamic ranges for each ground-truth value of these datasets are detailed in Table 1. These ranges were selected to be representative of the experimental values. Following [15], the real part of the refractive index of the dielectric material increases when submitted to a shock wave. The loss function in this stage is minimized by a standard gradient descent algorithm. Then, in the second stage, the predicted values from the ILSW-Net model are refined by minimizing the physics-informed MSE loss in the time domain using the Nelder–Mead algorithm.

Table 1. Dynamic range of ground-truth values used for the generation of training and validation datasets.

Ground Truth	Minimum Value	Maximum Value
Real part of the refractive index (n_1)	1	2
Imaginary part of the refractive index (n_1)	0.001	0.2
Real part of the refractive index (n_2)	1	3
Imaginary part of the refractive index (n_2)	0.001	0.2
Shock wavefront velocity (V_1)	2000 m/s	6000 m/s
Particle velocity (V_2)	200 m/s	600 m/s

3.2. Hyper-Parameter Setting

We initialize the model with He' normal initializer [16]. The model is trained for 400 epochs using an Adam optimizer [17]. The learning rate is dynamically adjusted via a learning rate scheduler with a reduced factor of 0.5, patience of 5 epochs, and a minimum learning rate of 0. An early stopping mechanism is also used to prevent overfitting by finishing the training if the training loss is not decreased within 10 epochs.

4. Results and Discussions

4.1. Lossless Material

In a previous study referenced [9], material losses were negligible, allowing us to consider the corresponding signal as normalized by Equation (2). Consequently, a comparison between our proposed model (ILSW-Net) and the model reported in [9] is conducted. More explicitly, both models are trained on normalized simulated signals, along with the real part of n_1, serving as the additional input, while velocities V_1 and V_2 and the real part of n_2 are the output variables. This comparison is based on the mean absolute percentage error (MAPE) of the models' predictions on the validation dataset. In Table 2, our proposed ILSW-Net model demonstrates lower MAPE values across all three dimensions (V_1, V_2, r_2) compared to the CNN model used in [9].

Table 2. The mean absolute percentage error (%) of ILSW-Net and the CNN model used in [9] for velocities V_1 and V_2 and the real part of n_2 on the validation set.

Model	V_1	V_2	r_2
Model [9]	2.46	3.59	0.75
ILSW-Net	0.68	1.37	0.5

4.2. Lossy Material

Since a two-stage training procedure is adopted to solve the inverse problem of a lossy shocked wavefront, in this section, we first report the performance of the ILSW-Net model on the simulated dataset, then present its application to the real-world signals.

4.2.1. Validation on Simulated Data

As mentioned earlier, the simulated data are used in both the validation and training phases of the learning process. We conduct experiments using the different combinations of algorithmic ingredients proposed in Section 2. This allows us to quantify the effect of the data normalization process and the use of the refractive index (n_1) in boosting the performance of ILSW-Net. The configurations to be explored are listed as follows:

- ILSW-Net with only the waveform as input (one-input ILSW-Net);
- One-input ILSW-Net with the data normalization process;
- ILSW-Net with two inputs, namely the waveform and the complex refractive index (n_1) (two-input ILSW-Net);
- Two-input ILSW-Net with the data normalization process.

Figure 2 shows the evolution of the training/validation loss during the learning procedure. We can see that in the first two configurations, when using only the waveform input (Figure 2a,b), the model cannot converge, with a high training loss at the end. When using the complex refractive index (n_1) as input (Figure 2c), the model can remarkably converge, with training loss reduced significantly. This demonstrates the impact of using n_1 in facilitating the learning of ILSW-Net. However, the validation loss is still very high compared to the training loss; this means that the model exhibits overfitting. Fortunately, by normalizing the data (Figure 2d), the two-input ILSW-Net is successfully optimized, with better convergence, no overfitting, and a more stable validation loss curve.

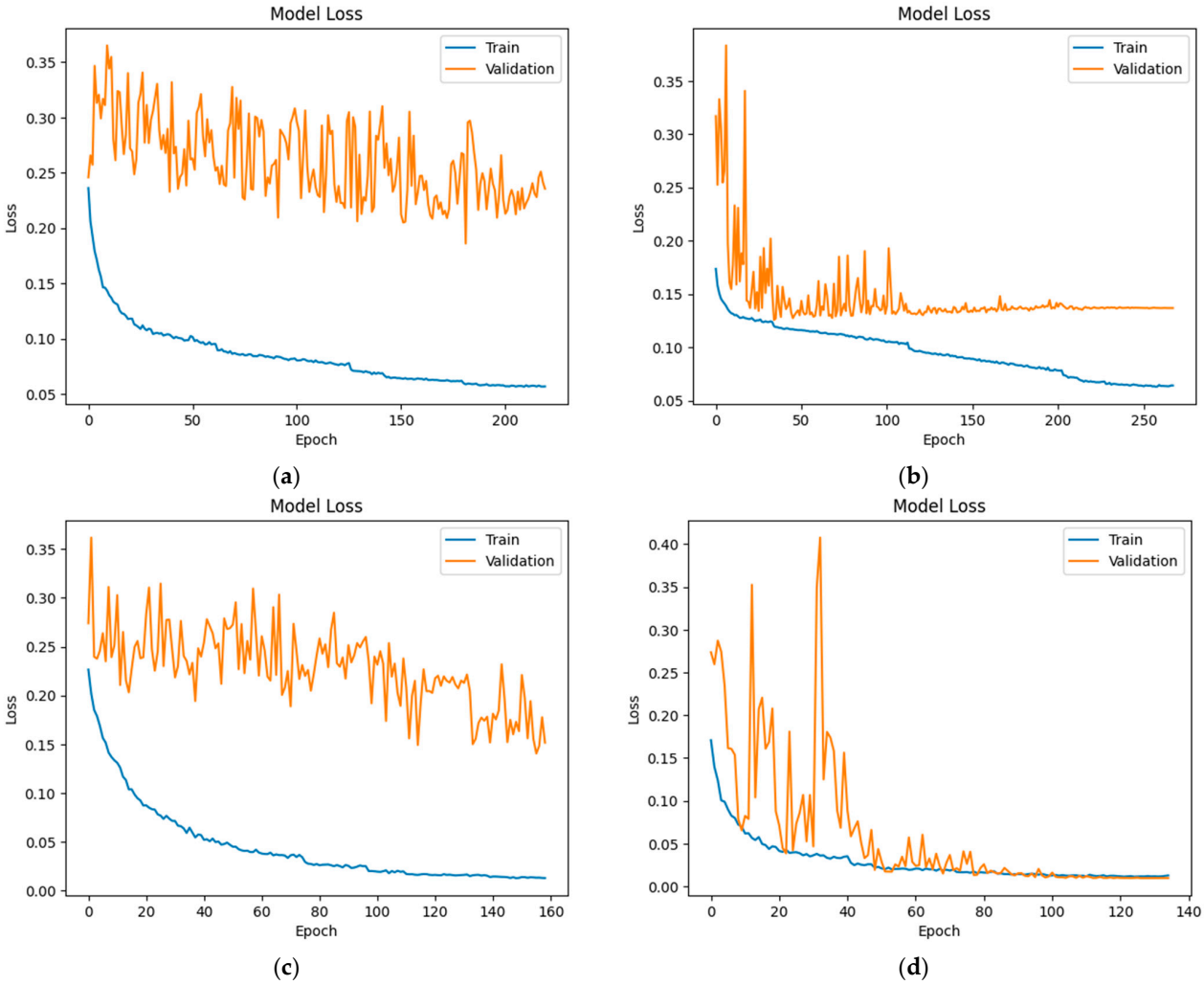

Figure 2. Performance comparison for different ILSW-Net configurations: (**a**,**b**) using a normalization (norm.) step; (**c**) using real and imaginary parts of the refractive index (n_1) as input; (**d**) using a norm. step and real and imaginary parts of the refractive index (n_1) as input.

The mean absolute percentage error (MAPE) of our model prediction on the validation dataset is reported in Table 3. We can see that by using both n_1 and the data normalization process, we can significantly reduce the MAPE from 14.59 to 0.69% (21×) for V_1, from 16.2 to 1.28% (13×) for V_2, and from 13.81 to 0.79% (17×) for r_2. However, the error of κ_2 is still large, although it is reduced from 70.65 to 16.95% (4×). These results are also visually demonstrated in Figure 3 with scatter plots of ground-truth prediction values. To investigate this result, the distribution of the κ_2 MAPE relative to its ground truth is explored. Figure 4 shows that the error is particularly high at low-ground-truth κ_2 values. In detail, for a ground-truth κ_2 smaller than 0.025, our model exhibits an MAPE of 33.41%,

while that for a ground-truth κ_2 larger than 0.025 is only 3.13%. This result suggests the use of another loss function (e.g., MAPE) to improve the performance of our model.

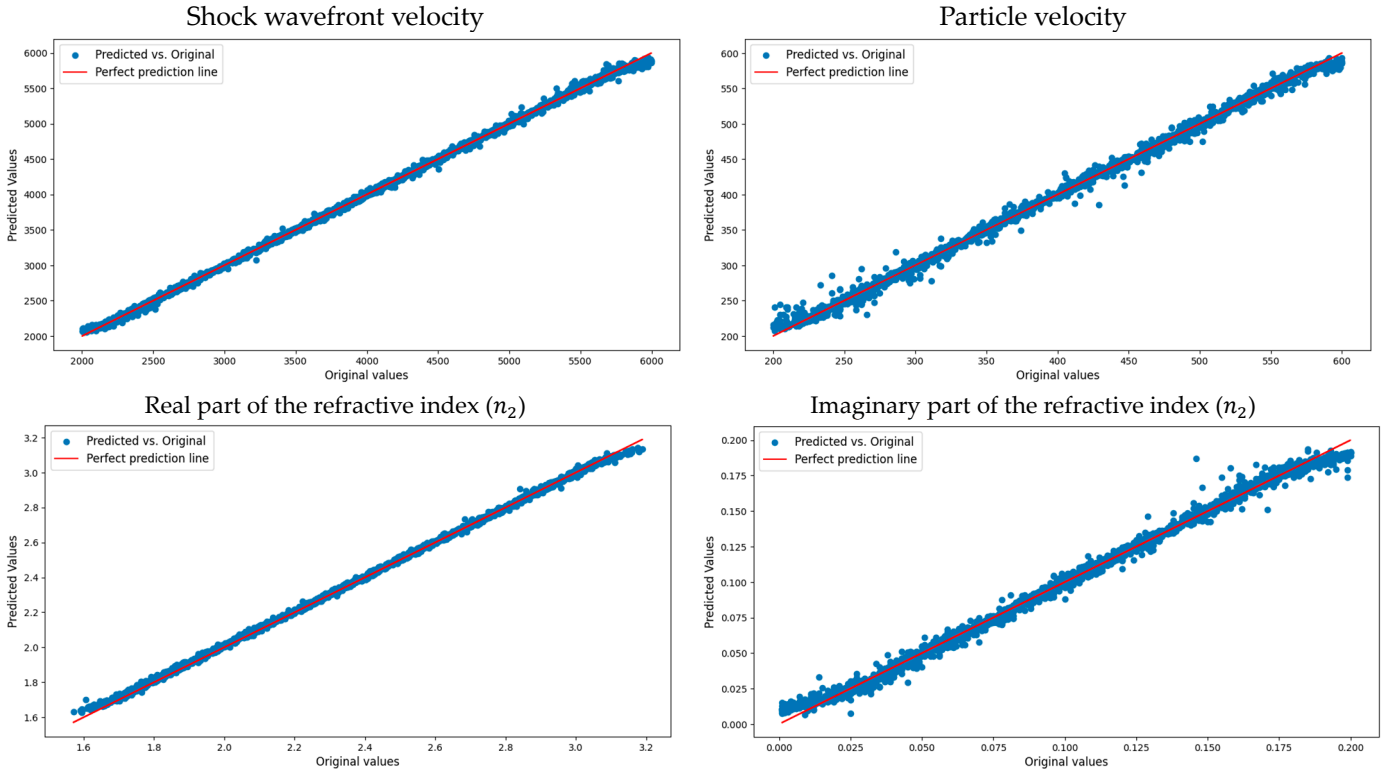

Figure 3. Scatter plot of four values, namely V_1, V_2, and the real part (r_2) and the imaginary part (κ_2) of the refractive index (n_2). The original values are depicted on x-axis, while predicted values are displayed on the y-axis.

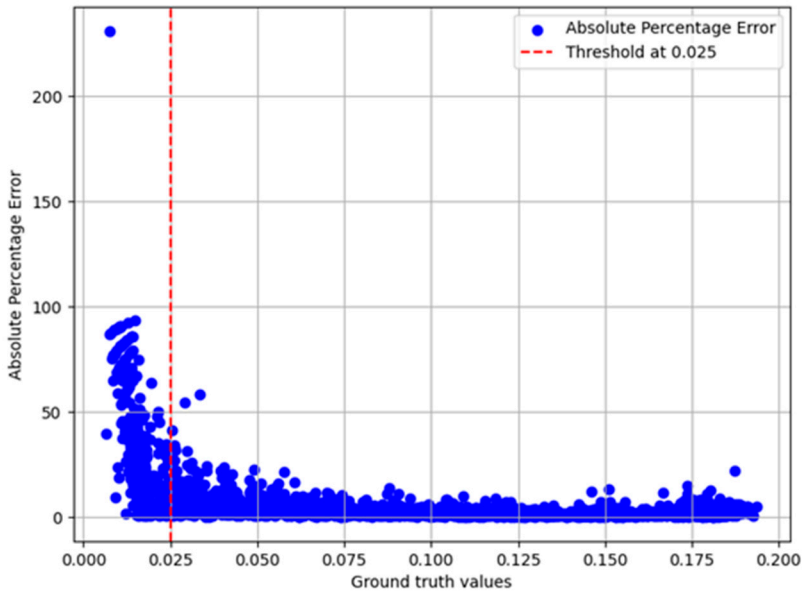

Figure 4. Distribution of ground-truth values of κ_2 and the corresponding absolute percentage error (on the y-axis).

Table 3. The mean absolute percentage error (%) of ILSW-Net for velocities V_1 and V_2 and the real/imaginary parts of n_2 on the validation set.

Method	V_1	V_2	r_2	κ_2
One-input ILSW-Net (baseline)	14.59	16.2	13.81	70.65
One-input ILSW-Net using norm. step	9.49	9.82	9.22	136.62
Two-input ILSW-Net	4.29	10.38	2.75	77.62
Two-input ILSW-Net using norm. step (final model)	0.69	1.28	0.79	16.95

4.2.2. Application to Experimental Data

The result obtained with real-world data is achieved after applying both the final model and the Nelder–Mead algorithm to two distinct physical waveforms delivered by a millimeter-wave (94 GHz) interferometer during a symmetrical shock experiment on high-density polyethylene (HDPE, $n_1 = 1.5 - 0.023i$) and polymethyl methacrylate (PMMA, $n_1 = 1.581 - 0.024i$) dielectric material samples. The impactor material is the same as the driver plate and the back plate of the target. The impactor is 90 mm in diameter and 10 mm thick. The driver plate is 110 mm in diameter and 15 mm thick, and the back plate is 80 mm in diameter and 25 mm thick. The impact velocity is measured with laser interferometry and less than 2% uncertainty.

First, the initial predictions (V_1, V_2, r_2, κ_2) are generated by ILSW-Net using the normalized physical signal and the real/imaginary parts of n_1 as two inputs. Then, they are refined by the Nelder–Mead algorithm, further enhancing their accuracy. In Figure 5, the graph serves as a visual guide for comparing the differences between the experimental waveform and the waveform calculated using known values of n_1, along with the predicted values of V_1, V_2, and n_2. It is shown clearly that the signal reconstructed using the final predictions from ILSW-Net and the optimization algorithm fit better with the original signal. The estimations of V_1, V_2, and complex n_2 are given in Table 4. The accuracy of ILSW-net is compared for V_1 and V_2 values obtained from the experiments. These values are calculated from the experimental impact velocities with hydrocode shock behavior numerical simulations. The impedance-matching method is applied with a Mie–Gruneisen equation of state for the materials [7]. Notably, the accuracy of V_1 and V_2 is increased after applying the optimization algorithm. These improvements may suggest a positive influence on the predicted values of the complex refractive index. The accuracy is better for the shock velocity than for the particle's velocity, which seems to be correlated with the original signal itself, with a higher number of periods for the high-frequency part of the double oscillations of the original signal and only one period for HDPE and half a period for PMMA samples.

Table 4. Estimation of V_1, V_2, and n_2 by ILSW-Net for both HDPE and PMMA dielectric materials under mechanical impact with or without application of the optimization method. The accuracy is obtained for V_1 and V_2 from the experiments, as deduced from the experimental impact velocities.

	HDPE		PMMA	
	Prediction	**Accuracy (%)**	**Prediction**	**Accuracy (%)**
V_1 without refinement	3616 m/s	99.06	3397 m/s	89.81
V_1 with refinement	3631 m/s	99.47	3375 m/s	90.40
V_2 without refinement	589 m/s	85.57	251 m/s	82.67
V_2 with refinement	565 m/s	89.20	270 m/s	88.93
Real$[n_2]$ without refinement	1.63		1.616	
Real$[n_2]$ with refinement	1.60		1.614	
Im$[n_2]$ without refinement	0.036		0.0232	
Im$[n_2]$ with refinement	0.031		0.0224	

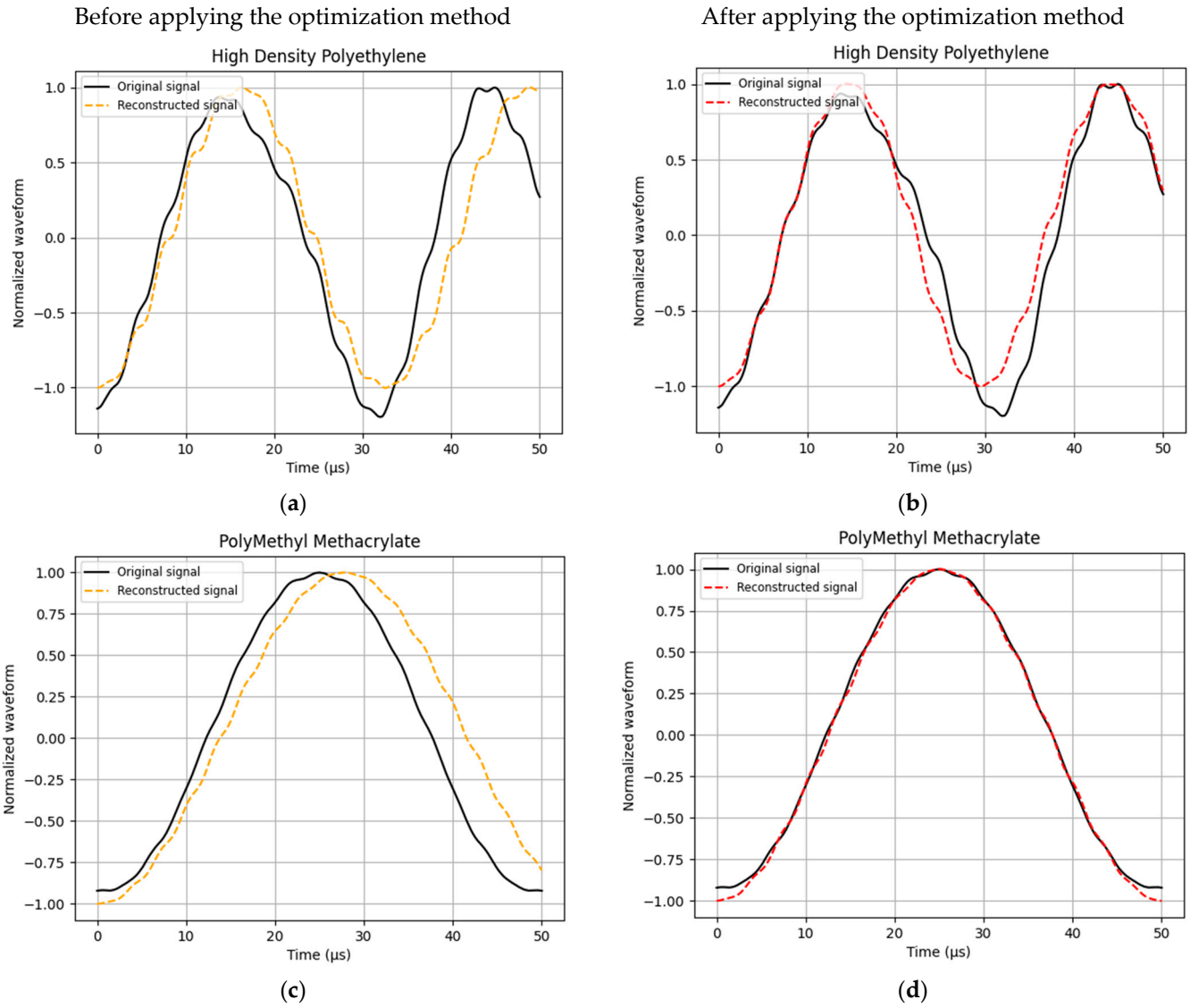

Figure 5. Comparison of theoretical waveforms (simulated using Equation (1), which accounts for the dielectric losses with the parameters given Table 4) with experimental waveforms delivered by a 94 GHz interferometer during impact experimentation. (**a**,**b**) High-density polyethylene (HDPE) material; (**c**,**d**) polymethyl methacrylate (PMMA) material.

5. Conclusions

In conclusion, our study demonstrates the relevance and effectiveness of the use of neural networks in conjunction with the Nelder–Mead algorithm for remote characterization of lossy dielectric materials subjected to a mechanical impact by a millimeter-wave (94 GHz) interferometer.

When applied to simulated waveforms, our results are promising, revealing a neural network mean absolute percentage error of approximately 1% for shock wavefront velocity, particle velocity, and the real part of the refractive index in shocked dielectric materials. The mean absolute percentage error is approximately 17% for the imaginary part of the refractive index in shocked dielectric materials. This accuracy shows the intrinsic ability of the proposed neural network to capture the subtle relationships between the input waveform and the real and imaginary parts of the complex refractive index of shocked materials. Furthermore, the proposed ILSW-Net provides an accurate estimation of the shock wavefront and particle velocities in shocked dielectric materials. High prediction performance on simulated waveforms validates the methodological approach that we

adopted in this and underlines the robustness of our model. When tested on measured waveforms delivered by a millimeter-wave interferometer, the use of a physics-informed loss optimized by the Nelder–Mead algorithm enables a better fit between the reconstructed signal and the original waveform in the time domain. Additionally, it improves accuracy for shock wavefront and particle velocities compared to experimental values.

In summary, this study reports, for the first time, the estimation of the complex refractive index of lossy dielectric materials under mechanical impact. Future work may involve the exploration of more robust deep learning model architectures, along with another loss function, to further improve the prediction performance, particularly in the case of the imaginary part of the refractive index (n_2).

Author Contributions: Conceptualization, H.A.; methodology, N.T.P., A.L. and H.A.; software, N.T.P.; validation, A.L. and H.A.; formal analysis, N.T.P.; investigation, N.T.P. and H.A.; data curation, N.T.P.; writing—original draft preparation, N.T.P.; writing—review and editing, A.L. and H.A.; supervision, A.L. and H.A.; project administration, A.L. and H.A; funding acquisition, A.L. All authors have read and agreed to the published version of the manuscript.

Funding: This research was funded by the CEA Gramat, France.

Institutional Review Board Statement: Not applicable.

Informed Consent Statement: Not applicable.

Data Availability Statement: The data presented in this study are available upon request from the corresponding author.

Conflicts of Interest: The authors declare no conflicts of interest. The funders had no role in the design of the study; in the collection, analyses, or interpretation of data; in the writing of the manuscript; or in the decision to publish the results.

References

1. Luther, G.G.; Warthen, B.J. Microwave interferometry to elucidate shock properties. *AIP Conf. Proc.* **1994**, *309*, 1755–1757.
2. Warthen, B.; Luther, G. *A Microwave Interferometer to Measure Transient Properties*; Technical Report; Los Alamos National Laboratory (LANL): Los Alamos, NM, USA, 1994.
3. Hawke, R.S.; Mitchell, A.C.; Keeler, R.N. Microwave measurement of permittivity and electrical conductivity in shock compressed liquids. *Rev. Sci. Instrum.* **1969**, *40*, 632–636. [CrossRef]
4. Glancy, B.C.; Krall, A.D. *Microwave Interferometric Measurements of Particle and Wave Velocities in Porous Media*; Technical Report; Naval Surface Warfare Center: Dahlgren, VA, USA, 1990.
5. Krall, A.D.; Glancy, B.C.; Sandusky, H.W. Microwave interferometry of shock wave. I. unreacting porous media. *J. Appl. Phys.* **1993**, *74*, 6322–6327. [CrossRef]
6. Glancy, B.C.; Sandusky, H.W.; Krall, A.D. Microwave interferometry of shock wave. II. reacting porous media. *J. Appl. Phys.* **1993**, *74*, 6328–6334. [CrossRef]
7. Rougier, B.; Aubert, H.; Lefrançois, A.; Barbarin, Y.; Luc, J.; Osmont, A. Reflection of Electromagnetic Waves on Moving Interfaces for Analyzing Shock Phenomenon in Solids. *RadioScience* **2018**, *53*, 888–894. [CrossRef]
8. Rougier, B.; Lefrançois, A.; Chuzeville, V.; Poeuf, S.; Aubert, H. Static and Dynamic Permittivity Measurement of High Explosives in the W band to investigate shock and detonation phenomena. *Propellants Explos. Pyrotech.* **2019**, *44*, 153–159. [CrossRef]
9. Mapas, J.; Lefrançois, A.; Aubert, H.; Comte, S.; Barbarin, Y.; Lavayssière, M.; Rougier, B.; Dore, A. Shock Properties Characterization of Dielectric Materials Using Millimeter-Wave Interferometry and Convolutional Neural Networks. *Sensors* **2023**, *23*, 4835. [CrossRef]
10. Kanakov, V.A.; Lupov, S.Y.; Orekhov, Y.I.; Rodionov, A.V. Techniques for retrieval of the boundary displacement data in gas-dynamic experiments using millimeter-waveband radio interferometers. *Radiophys. Quantum Electron.* **2008**, *51*, 210–221. [CrossRef]
11. Bel'skii, V.M.; Mikhailov, A.L.; Rodionov, A.V.; Sedov, A.A. Microwave diagnostics of shockwave and detonation processes. *Combust. Explos. Shock. Waves* **2011**, *47*, 639–650. [CrossRef]
12. He, K.; Zhang, X.; Ren, S.; Sun, J. Deep Residual Learning for Image Recognition. In Proceedings of the IEEE Conference on Computer Vision and Pattern Recognition (CVPR), Las Vegas, NV, USA, 27–30 June 2016; pp. 770–778.
13. Solovyev, R.; Vakhrushev, M.; Radionov, A.; Aliev, V.; Shvets, A. Deep Learning Approaches for Understanding Simple Speech Commands. In Proceedings of the 2020 IEEE 40th International Conference on Electronics and Nanotechnology (ELNANO), Kyiv, Ukraine, 22–24 April 2020; pp. 6–7.

14. Takenaga, S.; Ozaki, Y.; Onishi, M. Practical initialization of the Nelder–Mead method for computationally expensive optimization problems. *Optim. Lett.* **2023**, *17*, 283–297. [CrossRef]
15. Davison, L.; Graham, R.A. Shock compression of solids. *Phys. Rep.* **1979**, *55*, 255–379. [CrossRef]
16. He, K.; Zhang, X.; Ren, S.; Sun, J. Delving Deep into Rectifiers: Surpassing Human-Level Performance on ImageNet Classification. In Proceedings of the IEEE International Conference on Computer Vision (ICCV), Santiago, Chile, 7–13 December 2015; pp. 1026–1034.
17. Kingma, D.; Ba, J. ADAM: A Method for Stochastic Optimization. *arXiv* **2014**, arXiv:1412.6980.